THE JOURNAL OF PHYSICAL CHEMISTRY C

Article

Cite This: J. Phys. Chem. C 2019, 123, 19879−19886

pubs.acs.org/JPCC

Periodic Arrays of Dewetted Silver Nanostructures on Sapphire and Quartz: Effect of Substrate Truncation on the Localized Surface Plasmon Resonance and Near-Field Enhancement

Trevor B. Demille,[†] Robert A. Hughes,[†] and Svetlana Neretina*[,†,‡]

[†]College of Engineering and [‡]Department of Chemistry and Biochemistry, University of Notre Dame, Notre Dame, Indiana 46556, United States

Supporting Information

ABSTRACT: Substrate-supported plasmonic nanostructures are distinct from their colloidal counterparts, in that they are surrounded by an asymmetric dielectric environment composed of the substrate material and the surrounding ambient. Such environments inevitably lead to plasmonic resonances and near-fields that differ from those of solution-dispersed structures. The most straightforward method for fabricating substrate-based plasmonic nanostructures is through the solid-state dewetting of ultrathin films. This process typically leads to nanostructures with an asymmetric geometry due to an apparent truncation by the substrate to an otherwise symmetric structure. While changes to the plasmonic properties resulting from the substrate-imposed dielectric environment are well studied, a comprehensive understanding of the effect of substrate truncation is lacking. Here, a study of the plasmonic properties of substrate-truncated Ag nanospheres is presented, where, through experiment and simulation, the influence of substrate truncation on plasmonic resonances and the associated near-fields are elucidated. It is shown that increases to the degree of truncation give rise to a substantial red shift and strengthening of the dipole resonance, a weakening of the quadrupole resonance, and a strengthening of the near-field intensities near the nanostructure−substrate interface. The study contributes to the understanding needed to rationally design nanostructure−substrate systems for on-chip plasmonic devices.

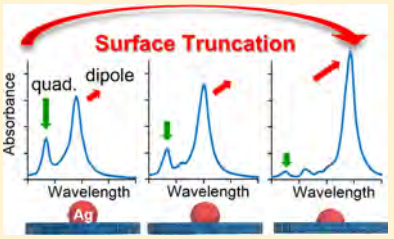

INTRODUCTION

The mere placement of a noble-metal nanostructure onto a substrate surface can radically alter its plasmonic response due to its high sensitivity to the adjacent dielectric environment.[1−5] Such environments profoundly differ from those experienced by colloidal nanostructures because the support is only in partial contact with nanostructures, whereas a colloid is enveloped in an isotropic dielectric medium.[6−9] The support can also be the recipient of hot electrons,[10] exposed to plasmonic heating,[11,12] alter chemical activity,[13] and promote coupling phenomena.[14] Through the controlled immobilization of plasmonic nanostructures at site-specific locations, the support can also facilitate the formation of nanogaps between adjacent structures that lead to the generation of plasmonic hot spots.[15] Such capabilities have been widely exploited to promote applications in the areas of catalysis,[13,16] surface-enhanced spectroscopy,[17,18] chemical and biological sensing,[18,19] and fluorescence.[20,21] The nanostructure−support combination, hence, gives rise to a unique set of opportunities that allow for both tunable plasmonic properties and an expanded list of functionalities.

Nanostructure supports can be categorized as planar or nonplanar, where the former is well suited to substrate-based device applications, while the latter is most commonly used as a retrievable structure for nanoscale catalysts.[22,23] Numerous methodologies have been devised to form plasmonic nanostructures on planar substrates in both random[24,25] and organized patterns.[26−28] Among these, the solid-state dewetting of ultrathin films and the directed dewetting of lithographically patterned films represent two of the most straightforward means for fabricating substrate-immobilized nanostructures where the placement on the substrate is randomized and arrayed, respectively. Dewetting occurs when an ultrathin metallic film is heated to high temperatures, causing it to agglomerate into a more energetically favorable configuration. Surface energy arguments based on the Winterbottom construction indicate that the lowest-energy configuration for a face-centered cubic metal is the Wulff shape, which is a substrate-truncated cuboctahedron enclosed by eight (111) and six (100) facets.[29,30] In practice, however, dewetted structures tend to deviate from the Wulff shape, often showing additional facets or appearing well rounded due to the intricacies of kinetic and thermodynamic factors. The precise shape of the dewetted nanostructures, as well as the degree of surface truncation, can also be influenced by numerous factors including substrate surface roughness,[31] the dewetting temperature,[32] the heteroepitaxial relationship between the substrate and metal,[33] substrate surface reconstructions,[34] and interface chemistry.[35] It is important to note that the degree of truncation, which for spherical structures is characterized by

Received: June 14, 2019
Revised: July 19, 2019
Published: July 22, 2019

DOI: 10.1021/acs.jpcc.9b05692
J. Phys. Chem. C 2019, 123, 19879−19886

the contact angle, influences the plasmonic response of supported structures.[4] This effect, in combination with the asymmetric dielectric environment resulting from the substrate,[1] leads to a plasmonic signature that is distinct from any structure formed through the colloidal synthesis.

Previously, we demonstrated a technique for fabricating periodic arrays of noble-metal nanostructures that utilized nanoimprint lithography (NIL) in combination with templated dewetting.[36,37] The so-formed structures are highly crystalline and appear as substrate-truncated nanospheres. Here, using both simulation and experiment, we examine the optical properties of Ag nanostructures formed on sapphire and quartz substrates where the emphasis is placed on defining the role that substrate truncation has on the plasmon resonance and the associated near-fields. It is shown that the structures exhibit two prominent plasmon resonance modes where a quadratic relationship exists between the ratio of the maximum absorbance for these two modes and the fraction of the sphere that is truncated. Moreover, it is shown that both the sharp geometry of the truncation plane and the polarizability of the Ag atoms at the metal−substrate interface play a decisive role in restricting electron oscillations near the interfacial plane and, as a result, lead to nanospheres with a higher degree of truncation having a greater electromagnetic near-field enhancement.

EXPERIMENTAL AND THEORETICAL METHODS

Materials. The 19 mm diameter target used to sputter-deposit Ag films was cut from a 0.25 mm thick foil with 99.9985% purity (Alfa Aesar). Two-side polished substrates with areal dimensions of 10 × 10.5 mm^2 were cut from [0001]-oriented wafers of sapphire (thickness = 0.65 mm, diameter = 100 mm) and quartz (thickness = 0.5 mm, diameter = 76 mm). The stamp and 7030R moldable thermal resist used in the NIL process were sourced from Lightsmyth Technologies and Micro Resist Technology GmbH, respectively. Ultrahigh purity Ar was used as the processing gas in the high-temperature-directed assembly of Ag nanostructures.

Nanostructure Fabrication. The NIL process, which is described in detail elsewhere,[37] imprints a hexagonal array of cylindrical rods (diameter = 240 nm, length = 350 nm, center-to-center distance = 600 nm) into a 425 nm thick moldable resist. The Ag film deposited through the openings in the resist has a thickness of 26 nm. After the lift-off procedure is complete, the Ag disc array is exposed to a heating regimen that sees it heated in a flowing Ar (30 sccm) to 965 °C in 19 min, after which the sample is cooled down to room temperature for over a 55 min period. During this procedure, the Ar flow is halted for temperatures above 800 °C so as to limit Ag evaporation. To achieve a range of nanosphere truncations, 5 nm thick Ag films were dewetted on substrate surfaces that were altered prior to film deposition using a reactive ion etching (RIE) procedure utilizing RF powers of 20 and 40 W and lasting between 25 and 75 s.

Simulations. Discrete dipole approximation (DDA) simulations were carried out using the DDSCAT 7.3 software package.[38] The technique represents a nanocrystal geometry, referred to as a target, as a finite three-dimensional cubic array of individually polarizable points whose properties are defined by the dielectric properties of the material. When subjected to an oscillating external electric field (i.e., light), each of these points acquires a dipole moment whose collective response allows for the scattering and absorption cross sections of the nanocrystal to be calculated. Target geometries are designed using the software package LAMMPS[39] and visualized using visual molecular dynamics.[40] For all simulations, the number of dipoles defining the Ag nanostructure (≈25 000) and substrate (≈65 000) was held constant to within 0.1%. The dielectric constants for Ag, sapphire, and quartz were taken from well-accepted sources.[41,42]

Instruments and Characterization. SEM images were obtained using a Magellan 400 FEI field emission scanning electron microscope using a secondary electron detector operating in an immersion mode. SEM tilt images were taken at 50° to the vertical and processed using ImageJ software. Absorbance spectra were acquired using a Jasco V-730 spectrophotometer. RIE utilized a SAMCO RIE-1C reactive ion etcher.

RESULTS AND DISCUSSION

Periodic Arrays of Substrate-Truncated Ag Nanospheres. Figure 1a shows a schematic of the procedure used to fabricate periodic arrays of substrate-truncated Ag nanospheres on quartz (SiO_2) and sapphire (Al_2O_3) substrates. The procedure uses NIL in combination with templated dewetting. Briefly, the substrate is spin-coated with a moldable polymeric resist that is then imprinted with a silicon stamp composed of a patterned array of nanoscale cylindrical columns. The stamp is then removed from the surface and exposed to a reactive ion

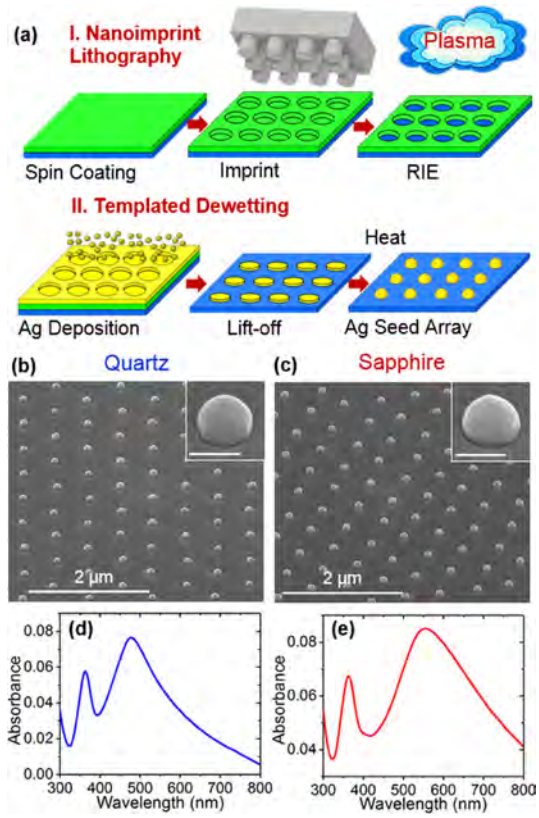

Figure 1. (a) Schematic of the nanofabrication method used to pattern periodic arrays of truncated Ag nanospheres on quartz and sapphire substrates. Tilted-view SEM images of arrays formed on (b) quartz and (c) sapphire substrates, where the insets show high-magnification images of a truncated sphere. Absorbance spectra for the Ag nanostructures formed on (d) quartz and (e) sapphire substrates. Scale bar for the insets is 100 nm.

DOI: 10.1021/acs.jpcc.9b05692
J. Phys. Chem. C 2019, 123, 19879−19886

etch whose purpose is to expose the substrate surface at the base of each imprinted column. A thin film of Ag is then deposited over the imprinted surface, after which a lift-off procedure is used that sees the resist dissolved and any metal on its surface washed away. The pattern of cylindrical polycrystalline Ag discs is then heated to high temperatures where each agglomerates to form a single highly crystalline nanostructure. The heating regimen used sees the nanostructure heated to temperatures slightly in excess of the Ag melting point followed by rapid cooling, a procedure that gives rise to nanostructures with the desired truncated sphere geometry.[43] Figure 1b,c shows SEM images of the structures formed on quartz and sapphire substrates, respectively. The structures appear as substrate-truncated nanospheres with average diameters of 116 nm for quartz and 110 nm for sapphire. For the purpose of this study, a truncation fraction (t_f) is defined as the fraction of the complete sphere diameter that is cut off by the substrate surface. The Ag structures shown in Figure 1b,c have t_f values of 0.15 and 0.17, respectively.

The UV−vis absorbance spectra for the arrayed structures are shown in Figure 1d,e. Each spectrum shows two prominent localized surface plasmon resonance (LSPR) peaks: a high-wavelength dipole peak and a low-wavelength quadrupole peak. A comparison of the peak positions reveals that, while the wavelength of the quadrupole resonance is nearly identical for nanostructures deposited on the two substrates, the dipole peak is red-shifted by 76 nm for the sapphire case. With the Ag structures having approximately the same average diameter for the two substrates, this red shift is attributed to the different dielectric environments presented by the adjacent substrate material (n_{quartz} = 1.54, $n_{sapphire}$ = 1.7). While the observed spectroscopic features are in agreement with prior work on substrate-immobilized Ag nanostructures,[44] they are in stark contrast to the spectra exhibited by colloidal Ag nanospheres, whose plasmonic signature is dominated by a single LSPR dipole peak.[9] The appearance of both a prominent dipole and quadrupole peak is, hence, another manifestation of a substrate-induced effect.

DDA Simulations of the Absorbance Spectra for Substrate-Truncated Ag Nanospheres. While the absorbance spectra in Figure 1d,e indicate that substrate-truncated Ag nanostructures have a plasmonic signature that is decidedly different from spherical colloids, an in-depth experimental analysis of these effects is difficult since a systematic variation of the degree of truncation over its entire range is infeasible. A comprehensive examination has therefore been carried out using DDA simulations in an effort to deconvolute the influences of nanostructure size, the degree of truncation, and variations to the index of refraction of the substrate. The calculations are validated with experimental data where possible.

Figure 2 shows DDA simulations of the absorbance spectra for Ag nanostructures immobilized on sapphire and quartz substrates for a range of diameters and for two different truncation fractions (t_f = 1/2, 1/5). The t_f = 1/2 spectra show three peaks where the most prominent is the dipole peak and the peak near 340 nm is the quadrupole peak. Both of these peaks are observed in the experimental data but are significantly broader. The weak central peak, which is indiscernible in experimental data, is likely attributable to a substrate-induced Fano resonance.[45,46] The t_f = 1/5 spectra also show a prominent dipole and quadrupole peak but where the central peak is obscured by the dipole resonance. As is the

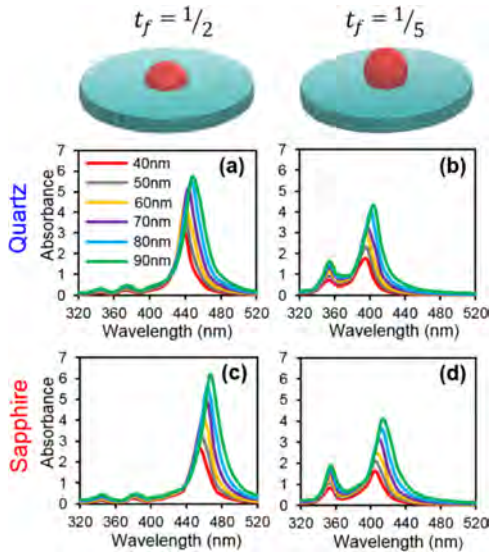

Figure 2. DDA simulations of the absorbance spectra for substrate-truncated Ag nanostructures with varying diameters (40−90 nm) and truncation fractions (t_f) of 1/2 and 1/5 resting on (a, b) quartz and (c, d) sapphire substrates.

case for colloidal structures, an increase in a nanostructure diameter leads to an increased absorbance and a red shift in the resonant frequency but where the shift is to a lesser degree for the quadrupole resonances. As expected, the spectra for identical nanostructures resting on different substrate materials have similar features except that the plasmon resonances are red-shifted for the sapphire case, a result that is attributable to its larger index of refraction.[47] The most substantial differences observed are associated with changes to the truncation fraction. A comparison of equivalent spectra reveals that smaller values give rise to (i) a substantial blue shift in the dipole resonance, (ii) a lower dipole absorbance, and (iii) a strengthening of the quadrupole mode.

With the LSPR spectra showing a high sensitivity to the truncation fraction, further simulations were performed to provide a more in-depth understanding of this parameter. Figure 3 shows the normalized absorbance spectra for 70 nm diameter Ag nanostructures where the truncation fraction is varied from 1/5 (i.e., nearly spherical) to 1/2 (i.e., hemispherical) for structures on sapphire and quartz, as well as those that are freestanding. Simulations for t_f > 1/2 can be found in the Supporting Information (Figure S1) but are excluded from Figure 3 because they are experimentally observed neither in this study nor in the literature. As the degree of truncation is increased over its range, the dipole peak for nanostructures on both substrates shifts from a value near 360 nm to one in excess of 440 nm. While it may seem counterintuitive that the dipole resonance of the smallest volume structure (i.e., hemispherical, t_f = 1/2) is red-shifted relative to the largest volume structure (i.e., nearly spherical, t_f = 1/5), the result is as expected if it is understood that for a substrate-bound structure, the dipole resonance occurs close to the interface where the in-plane radial dimensions of the hemisphere are much larger than a nearly spherical structure. It is these larger dimensions that lead to a higher-wavelength resonance. A comparison of the sapphire, quartz, and freestanding cases for any given truncation, as expected, reveals dipole resonances that become increasingly red-shifted as the index of refraction of the adjacent medium is increased.

DOI: 10.1021/acs.jpcc.9b05692
J. Phys. Chem. C 2019, 123, 19879−19886

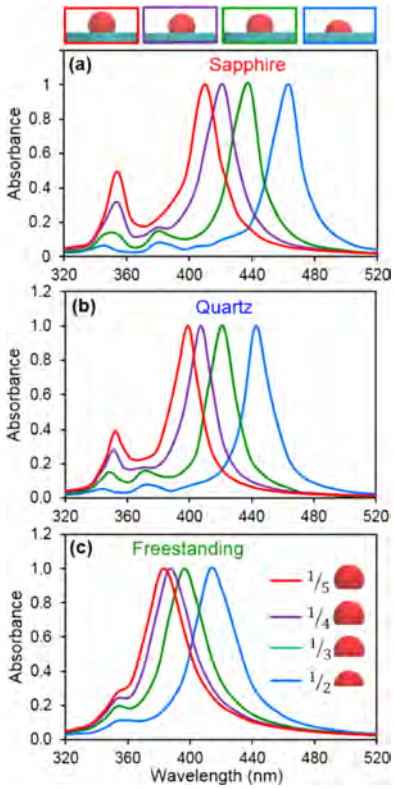

Figure 3. DDA simulations of the normalized absorbance spectra for Ag nanostructures with various truncation fractions (t_f = 1/5−1/2) that are resting on (a) sapphire and (b) quartz substrates and that are (c) freestanding.

If, however, a comparison is made of the degree to which the spectra blue-shift as t_f values are increased from 1/5 and 1/2, then values of 29, 44, and 54 nm are found for the freestanding, quartz, and sapphire cases, respectively. This shows that the degree of blue shift in the dipolar LSPR is bolstered by substrate supports having a higher index of refraction. This conclusion is in agreement with the experimental data shown in Figure 1d,e.

An examination of the quadrupole peak near 350 nm in Figure 3a−c reveals that it is relatively insensitive to changes in the index of refraction. All three cases show that, as the degree of truncation is decreased, the quadrupole peak shows a slight red shift and a gain in intensity relative to the dipole peak. The latter is of significance because it suggests that there exists a relationship between the ratio of these peak intensities (R = A_{dipole}/A_{quad}) and the truncation fraction. An examination of the nanostructure size-dependent absorbance data in Figure 2 reveals that R is independent of nanostructure size, a result that adds further significance to this parameter. R is, however, sensitive to the dielectric environment provided by the underlying substrate and, as such, its value is unique to a given substrate material. Figure 4a shows a plot of R vs t_f for Ag nanostructures deposited on quartz and sapphire substrates. The individual points were calculated by averaging the values obtained for nanostructures with diameters of 40, 50, 60, 70, 80, and 90 nm, where the standard deviation for any point is less than the diameter of the symbol used to plot the data. The dotted lines show a quadratic fit to the data. While it is difficult to experimentally vary the t_f value obtained for a specific substrate material, some variation is made possible by exposing the substrate surface to a reactive ion etch (RIE) prior to Ag deposition and dewetting. For any given RIE-treated sample, the R value was then obtained spectroscopically, while the t_f value was obtained through an examination of SEM images taken of 30 different structures. Figure 4b shows the four experimental data points obtained for nanostructures on each substrate material overlaid on the quadratic fit obtained through DDA simulation where the axes have been adjusted to highlight the region of interest. The fact that the experimental and theoretical results are in good agreement indicates that an accurate measure of the truncation fraction can be made solely based on spectroscopic measurements.

The mechanistic origin of the quadratic relationship between t_f and R (Figure 4a) can be derived from the governing equations for the dipole and quadrupole resonance modes. With the understanding that the path length, density, and geometric cross-sectional variables are identical for the absorbance expressions describing both the dipole and quadrupole modes, these variables cancel when taking the ratio R, leaving the following progression

$$R = \frac{A_{dipole}}{A_{quad}} = \frac{(C_{abs})_{dipole}}{(C_{abs})_{quad}} = \frac{\lambda_2 \mathrm{Im}(\bar{\alpha}_1)}{\lambda_1 \mathrm{Im}(\bar{\alpha}_2)} \quad (1)$$

Here, A, C_{abs}, $\lambda_{1,2}$, and $\bar{\alpha}_{1,2}$ are the absorbance, absorbance cross section, wavelength of the incident light at the resonant frequency, and bulk polarizability, respectively, where the subscripts denote the dipole (l = 1) and quadrupole modes (l = 2) of the truncated nanosphere. For the case of a full-freestanding sphere, the multipolar polarizability ($\bar{\alpha}_l$) scales like r_{sph}^{2l+1}.[48,49] The polarizability of a mode can, hence, be

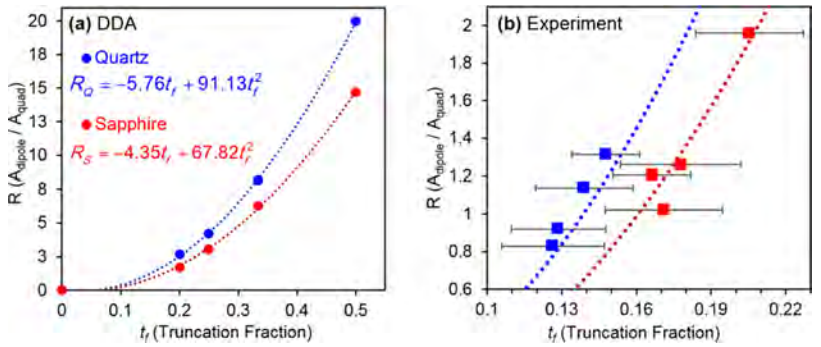

Figure 4. Plots of the ratio of the dipole-to-quadrupole absorbance versus the truncation fraction as obtained from (a) DDA simulations and (b) experiment. The dotted lines for both plots are the quadratic fits to the simulated data points. The error bars in (b) represent standard deviations.

DOI: 10.1021/acs.jpcc.9b05692
J. Phys. Chem. C 2019, 123, 19879−19886

expressed as the product of its bulk dielectric $D(\varepsilon_{med}, \kappa_l, \varepsilon_{Ag})$ and geometric $G(r_{sph},l)$ components

$$\bar{\alpha}_l = \frac{\varepsilon_{Ag,l} - \varepsilon_{med,l}}{\varepsilon_{Ag,l} + \kappa_l \varepsilon_{med,l}} r_{sph}^{2l+1} = D(\varepsilon_{med}, \kappa_l, \varepsilon_{Ag}) G(r_{sph}, l) \quad (2)$$

where r_{sph} represents the radius of the full sphere, $\varepsilon_{Ag,l}$ and $\varepsilon_{med,l}$ denote the dielectric constants of Ag and the ambient medium at the resonant wavelength of the dipole (l = 1) or quadrupole mode (l = 2), respectively, and κ_l is a mode-dependent shape factor.[50] When truncation is introduced, spherical symmetry is lost and $G(r_{sph,l})$ is altered with respect to that of a full-freestanding sphere.[51] This alteration, however, merely takes the form of a scalar multiplicative factor that can be expressed as a function of t_f. The geometric component for a truncated sphere can therefore be expressed as

$$G(r_{sph}, l) = r_{sph}^{2l+1} \sqrt{-4t_f^2 + 2t_f + 1} \quad (3)$$

Substituting eq 3 and the value for $D(\varepsilon_{med}, \kappa_l, \varepsilon_{Ag})$ into eq 1 and then rearranging the expression so that like terms, which result from quantities identical for both the dipole and quadrupole modes, are canceled out gives

$$R = \mathrm{Im}\left\{\frac{\varepsilon_{Ag,1} - \varepsilon_{med,1}}{\varepsilon_{Ag,2} - \varepsilon_{med,2}}\right\} \cdot \mathrm{Im}\left\{\frac{\varepsilon_{Ag,2} + \kappa_2 \varepsilon_{med,2}}{\varepsilon_{Ag,1} + \kappa_1 \varepsilon_{med,1}}\right\} \cdot \frac{\lambda_2}{\lambda_1 r_{sph}^2} \quad (4)$$

An examination of the two imaginary terms in eq 4 reveals that the first is a scalar quantity and the second is dependent on the mode-dependent shape factors κ_1 and κ_2. Such factors represent the ease by which available electrons can be polarized for a given nanostructure geometry and mode. Recognizing that the circular metal−substrate interface dominates the dampening effects of the ambient medium (vide infra), it is reasonable to presume that the radius of the metal−substrate interface, r_{int}, can be treated as the characteristic dimension for the shape factors. Based on geometrical considerations, an expression for r_{int} in terms of t_f is given by

$$r_{int} = 2r_{sph}\sqrt{t_f - t_f^2} \quad (5)$$

If dimensional consistency is to be maintained, then the geometric factors κ_1 and κ_2 must scale with r_{int} according to r_{int}^{2l+1} as was the case for a full-freestanding sphere. With the understanding that $\kappa_1 \propto r_{int}^3$ and $\kappa_2 \propto r_{int}^5$ and taking into account the magnitude of the r_{int} and $\varepsilon_{Ag,2}$ values of relevance to Figure 4, the approximations $\varepsilon_{Ag,2} \ll \kappa_2 \varepsilon_{med,2}$ and $\varepsilon_{Ag,1} \ll \kappa_1 \varepsilon_{med,1}$ can be applied to eq 4 to yield

$$R = A_0 \frac{\lambda_2}{\lambda_1} \cdot \frac{r_{int}^2}{r_{sph}^2} = A_0 \frac{\lambda_2}{\lambda_1} \cdot (t_f - t_f^2) \quad (6)$$

where the product of all scalar values has been set to A_0. Of importance is that eq 6 takes the form of the fits to the data shown in Figure 4a.

DDA Simulations of the Near-Fields for Substrate-Truncated Ag Nanospheres. Figure 5 compares the simulated near-fields of a freestanding Ag nanostructure to those that are resting on quartz and sapphire substrates for t_f values of 1/2 and 1/5 and a nanostructure diameter of 70 nm. The color maps correspond to cross sections taken through the center of the structure for a plane that is perpendicular to the truncation plane where the $|E/E_0|^2$ values are those occurring at the dipolar resonant wavelength for any given structure.

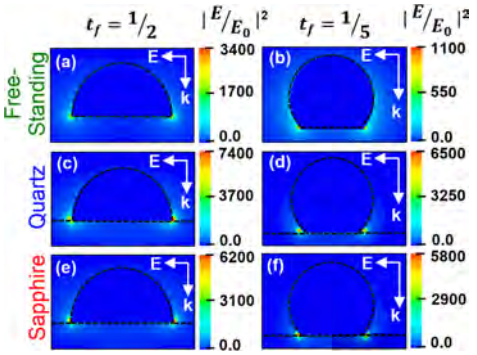

Figure 5. Simulations of the near-field enhancements for Ag nanostructures with two different truncations (t_f = 1/2 and 1/5) that are (a, b) freestanding and resting on (c, d) quartz and (e, f) sapphire substrates. Note that the diameter of all structures is 70 nm even though they are plotted on different scales for the sake of clarity.

Collectively, the simulations show that the maximum near-field intensities (i.e., hot spots) occur at the truncation plane but where higher intensities are observed when a substrate is present. Also apparent is that for all three cases the largest hot-spot intensity occurs for the structure with the highest degree of truncation (i.e., t_f = 1/2). Two additive influences are responsible for the observed trends. The first is that near-fields tend to concentrate at points of high curvature[52] and, with higher t_f values showing higher curvatures at the truncation plane edge, this effect, which is most readily apparent for freestanding structures (Figure 5a,b), becomes increasingly exaggerated as the truncation is increased. The second is that the dielectric environment of the substrate promotes electron oscillations near its surface.[53] This can be understood in terms of the Clausius−Mossotti relation,[54,55] discretized here with respect to the DDA framework, can be used to describe the polarizability of each individually polarizable point as

$$\alpha_i = \varepsilon_0 V_i \frac{(\varepsilon - \varepsilon_{med,i})}{(\varepsilon + B\varepsilon_{med,i})} \quad (7)$$

where ε_0 is the permittivity of free space, ε is the dielectric function of Ag, $\varepsilon_{med,i}$ is the dielectric constant of the surrounding medium for the ith subvolume V_i of the DDA model, and B is a geometric factor. From this equation, it can be seen that Ag atoms occupying the metal−substrate interface will have the greatest response to an incident electric field (i.e., light) because of increased polarizability resulting from larger differences in the dielectric functions of the two materials. As a result, plasmonic oscillations tend to occur at the metal−substrate interface, an effect that is seen even for spherical nanostructures (i.e., t_f = 0).[53] Based on these arguments, it is somewhat surprising that the Ag structures on quartz have more intense near-fields than those on sapphire even though the dielectric constant of quartz is lower. The full DDA framework can, however, account for this, in that progressively larger substrate dielectric constants, while giving rise to increased polarizability, also lead to light scattering becoming a more dominant process than absorbance, an effect that weakens the near-fields. This effect was previously described by El-Sayed and co-workers[56] when simulating the properties of Ag nanocubes on various substrate materials. The near-fields associated with the quadrupole peak (Figure S2) are considerably weaker for all three cases where the enhancement is greatest for the freestanding structure.

DOI: 10.1021/acs.jpcc.9b05692
J. Phys. Chem. C 2019, 123, 19879−19886

Broader Implications. The increasing interest in on-chip plasmonic devices underscores the importance of having a fundamental understanding of the interactions occurring when noble-metal nanostructures are brought into contact with substrate materials. The resulting adjustments to the plasmon resonances and near-fields are both significant and unavoidable. The use of substrate-immobilized structures derived from dewetting further complicates the situation through an apparent substrate-induced truncation that further convolutes the overall plasmonic response. This response, which is now being rigorously examined through optical[57] and electron energy loss spectroscopies,[43,58,59] if well understood and controllably manipulated, provides additional control for the rational design of nanostructure architectures with tunable plasmonic properties. One of the key stumbling blocks in achieving such control is that the degree of truncation is not readily varied since it is largely determined by the free surface energies of the substrate and metal (i.e., Young's equation). Methods are, however, becoming increasingly available that reshape dewetted nanostructures by promoting the formation of facets through exposure to liquid-phase chemistry[26,60] or kinetically driven vapor-phase[61] processes that lead to thermodynamically unfavorable configurations. Such processes offer the opportunity to alter and manipulate the truncation plane where the nanostructure and substrate intersect. The use of liquid-phase syntheses also offers the opportunity to realize more sophisticated nanostructure geometries such as core–shell,[62,63] core–void–shell,[64] and hollowed architectures,[65] where, in each case, the plasmonic signature is rendered unique due to the truncation plane induced by the dewetting process. The work described herein lays the groundwork for understanding these more sophisticated geometries.

CONCLUSIONS

In summary, we have demonstrated that the plasmonic response of Ag nanostructures is highly sensitive to an apparent truncation that occurs during the solid-state dewetting of ultrathin Ag films. Substrate-truncated nanostructures are shown to exhibit prominent dipole and quadrupole resonances where increases to the degree of truncation lead to a substantial red shift in the dipole mode. The ratio of the maximum absorbance for these two modes follows a quadratic relationship that is validated through simulation, experiment, and first principles. Increased truncation is also shown to give rise to near-field enhancements resulting from higher nanostructure curvatures at the truncation plane edge and the larger nanostructure–substrate contact area occurring as the nanostructure approaches a hemispherical geometry. The work, hence, contributes to the fundamental understanding needed to advance the use of substrate-immobilized nanostructures in photonic and optoelectronic devices.

ASSOCIATED CONTENT

Supporting Information

The Supporting Information is available free of charge on the ACS Publications website at DOI: 10.1021/acs.jpcc.9b05692.

Simulations showing that the trends observed in Figures 3 and 4 continue for truncation fractions greater than 1/2 (Figure S1); and simulations of the plasmonic near-fields associated with the quadrupole resonance (Figure S2) (PDF)

AUTHOR INFORMATION

Corresponding Author

*E-mail: sneretina@nd.edu.

ORCID

Svetlana Neretina: 0000-0002-6889-4384

Notes

The authors declare no competing financial interest.

ACKNOWLEDGMENTS

This work is supported by a National Science Foundation Award (DMR-1707593). The authors have benefited from the facilities available through the Notre Dame Integrated Imaging Facility (NDIIF).

REFERENCES

(1) Wiley, B. J.; Im, S. H.; Li, Z. Y.; McLellan, J.; Siekkinen, A.; Xia, Y. Maneuvering the Surface Plasmon Resonance of Silver Nanostructures through Shape-Controlled Synthesis. *J. Phys. Chem. B* **2006**, *110*, 15666–15675.

(2) Jain, P. K.; Huang, X.; El-Sayed, M. A.; El-Sayed, I. H. Review of Some Interesting Surface Plasmon Resonance-Enhanced Properties of Noble Metal Nanoparticles and Their Applications to Biosystems. *Plasmonics* **2007**, *2*, 107–118.

(3) Huang, X.; Lou, C.; Zhang, H. Experimentally Demonstrating Plasmonic Lattice Mode in Periodic Ag Nanoparticle Arrays on Quartz Trapezoidal Pillars. *J. Phys. D: Appl. Phys.* **2018**, *51*, No. 465101.

(4) Malinsky, M. D.; Kelly, K. L.; Schatz, G. C.; Van Duyne, R. P. Nanosphere Lithography: Effect of Substrate on the Localized Surface Plasmon Resonance Spectrum of Silver Nanoparticles. *J. Phys. Chem. B* **2001**, *105*, 2343–2350.

(5) Mahmoud, M. A.; El-Sayed, M. A. Substrate Effect on the Plasmonic Sensing Ability of Hollow Nanoparticles of Different Shapes. *J. Phys. Chem. B* **2013**, *117*, 4468–4477.

(6) Perassi, E. M.; Hrelescu, C.; Wisnet, A.; Döblinger, M.; Scheu, C.; Jäckel, F.; Coronado, E. A.; Feldmann, J. Quantitative Understanding of the Optical Properties of a Single, Complex-Shaped Gold Nanoparticle from Experiment and Theory. *ACS Nano* **2014**, *8*, 4395–4402.

(7) Mahmoud, M. A.; Chamanzar, M.; Adibi, A.; El-Sayed, M. A. Effect of the Dielectric Constant of the Surrounding Medium and the Substrate on the Surface Plasmon Resonance Spectrum and Sensitivity Factors of Highly Symmetric Systems: Silver Nanocubes. *J. Am. Chem. Soc.* **2012**, *134*, 6434–6442.

(8) Hooshmand, N.; Bordley, J. A.; El-Sayed, M. A. The Sensitivity of the Distance Dependent Plasmonic Coupling between Two Nanocubes to their Orientation: Edge-to-Edge versus Face-to-Face. *J. Phys. Chem. C* **2016**, *120*, 4564–4570.

(9) Cobley, C. M.; Skrabalak, S. E.; Campbell, D. J.; Xia, Y. Shape-Controlled Synthesis of Silver Nanoparticles for Plasmonic and Sensing Applications. *Plasmonics* **2009**, *4*, 171–179.

(10) Zhang, Y.; He, S.; Guo, W.; Hu, Y.; Huang, J.; Mulcahy, J. R.; Wei, W. D. Surface-Plasmon-Driven Hot Electron Photochemistry. *Chem. Rev.* **2018**, *118*, 1927–2954.

(11) Wang, D.; Koh, Y. R.; Kudyshev, Z. A.; Maize, K.; Kildishev, A. V.; Boltasseva, A.; Shalaev, V. M.; Shakouri, A. Spatial and Temporal Nanoscale Plasmonic Heating Quantified by Thermoreflectance. *Nano Lett.* **2019**, *19*, 3796–3803.

(12) Szymanski, P.; Mahmoud, M. A.; El-Sayed, M. A. The Last Step in Converting the Surface Plasmonic Energy into Heat by Nanocages and Nanocubes on Substrates. *Small* **2013**, *9*, 3934–3938.

(13) Devi, L. G.; Kavitha, R. A Review on Plasmonic Metal-TiO_2 composite for Generation, Trapping, Storing and Dynamic Vectorial Transfer of Photogenerated Electrons across the Schottky Junction in a Photocatalytic System. *Appl. Surf. Sci.* **2016**, *360*, 601–622.

DOI: 10.1021/acs.jpcc.9b05692
J. Phys. Chem. C 2019, 123, 19879–19886

(14) Zhang, S.; Xu, H. Optimizing Substrate-Mediated Plasmon Coupling toward High-Performance Plasmonic Nanowire Waveguides. *ACS Nano* **2012**, *6*, 8128−8135.
(15) Yang, Y.; Gu, C.; Li, J. Sub-5 nm Metal Nanogaps: Physical Properties, Fabrication Methods, and Device Applications. *Small* **2019**, *15*, No. 1804177.
(16) Sun, M.; Xu, H. A Novel Application of Plasmonics: Plasmon-Driven Surface-Catalyzed Reactions. *Small* **2012**, *8*, 2777−2786.
(17) Demirel, G.; Usta, H.; Yilmaz, M.; Celik, M.; Alidagi, H. A.; Buyukserin, F. Surface-Enhanced Raman Spectroscopy (SERS): An Adventure from Plasmonic Metals to Organic Semiconductors as SERS Platforms. *J. Mater. Chem. C* **2018**, *6*, 5314−5335.
(18) Li, M.; Cushing, S. K.; Wu, N. Plasmon−Enhanced Optical Sensors: A Review. *Analyst* **2015**, *140*, 386−406.
(19) Willets, K. A.; Van Duyne, R. P. Localized Surface Plasmon Resonance Spectroscopy and Sensing. *Annu. Rev. Phys. Chem.* **2007**, *58*, 267−297.
(20) Yu, H.; Rao, B.; Jiang, W.; Yang, S.; Zhu, M. The Photoluminescent Metal Nanoclusters with Atomic Precision. *Coord. Chem. Rev.* **2019**, *378*, 595−617.
(21) Shang, L.; Dong, S.; Nienhaus, G. U. Ultra-Small Fluorescent Metal Nanoclusters: Synthesis and Biological Applications. *Nano Today* **2011**, *6*, 401−418.
(22) Munnik, P.; de Jongh, P. E.; de Jong, K. P. Recent Developments in the Synthesis of Supported Catalysts. *Chem. Rev.* **2015**, *115*, 6687−6718.
(23) Demille, T. B.; Hughes, R. A.; Preston, A. S.; Adelung, R.; Mishra, Y. M.; Neretina, S. Light-Mediated Growth of Noble Metal Nanostructures (Au, Ag, Cu, Pt, Pd, Ru, Ir, Rh) From Micro- and Nanoscale ZnO Tetrapodal Backbones. *Front. Chem.* **2018**, *6*, No. 411.
(24) Farzinpour, P.; Sundar, A.; Gilroy, K. D.; Eskin, Z. E.; Hughes, R. A.; Neretina, S. Altering the Dewetting Characteristics of Ultrathin Gold and Silver Films using a Sacrificial Antimony Layer. *Nanotechnology* **2012**, *23*, No. 495604.
(25) Krishna, H.; Shirato, N.; Favazza, C.; Kalyanaraman, R. Pulsed Laser Induced Self-Organization by Dewetting of Metallic Films. *J. Mater. Res.* **2011**, *26*, 154−169.
(26) Hughes, R. A.; Menumerov, E.; Neretina, S. When Lithography Meets Self-Assembly: A Review of Recent Advances in the Directed Assembly of Complex Metal Nanostructures on Planar and Textured Surfaces. *Nanotechnology* **2017**, *28*, No. 282002.
(27) Ni, S.; Isa, L.; Wolf, H. Capillary Assembly as a Tool for the Heterogeneous Integration of Micro- and Nanoscale Objects. *Soft Matter* **2018**, *14*, 2978−2995.
(28) Roberts, N. A.; Fowlkes, J. D.; Mahady, K.; Afkhami, S.; Kondic, L.; Rack, P. D. Directed Assembly of One- and Two-Dimensional Nanoparticle Arrays from Pulsed Laser Induced Dewetting of Square Waveforms. *ACS Appl. Mater. Interfaces* **2013**, *5*, 4450−4456.
(29) Bao, W.; Jiang, W.; Srolovitz, D. J.; Wang, Y. Stable Equilibria of Anisotropic Particles on Substrates: A Generalized Winterbottom Construction. *SIAM J. Appl. Math.* **2017**, *77*, 2093−2118.
(30) Winterbottom, W. L. Equilibrium Shape of a Small Particle in Contact with a Foreign Substrate. *Acta Metall.* **1967**, *15*, 303−310.
(31) Gilroy, K. D.; Puibasset, J.; Vara, M.; Xia, Y. On the Thermodynamics and Experimental Control of Twinning in Metal Nanocrystals. *Angew. Chem., Int. Ed.* **2017**, *56*, 8647−8651.
(32) Thompson, C. V. Solid-State Dewetting of Thin Films. *Annu. Rev. Mater. Res.* **2012**, *42*, 399−434.
(33) Devenyi, G. A.; Li, J. F.; Hughes, R. A.; Shi, A. C.; Mascher, P.; Preston, J. S. Epitaxially Driven Formation of Intricate Supported Gold Nanostructures on a Lattice-Matched Oxide Substrate. *Nano Lett.* **2009**, *9*, 4258−4263.
(34) Silly, F.; Powell, A. C.; Martin, M. G.; Castell, M. R. Growth Shapes of Supported Pd Nanocrystals on $SrTiO_3$ (001). *Phys. Rev. B* **2005**, *72*, No. 165403.
(35) Hajjar, S.; Garreau, G.; Josien, L.; Bubendorff, J. L.; Berling, D.; Mehdaoui, A.; Pirri, C.; Maroutian, T.; Renard, C.; Bouchier, D.; et al. Morphology and Composition of Au Catalysts on Ge(111) Obtained by Thermal Dewetting. *Phys. Rev. B* **2011**, *84*, No. 125325.
(36) Preston, A. S.; Hughes, R. A.; Demille, T. B.; Rey Davila, V. M.; Neretina, S. Dewetted Nanostructures of Gold, Silver, Copper, and Palladium with Enhanced Faceting. *Acta Mater.* **2019**, *165*, 15−25.
(37) Menumerov, E.; Golze, S. D.; Hughes, R. A.; Neretina, S. Arrays of Highly Complex Noble Metal Nanostructures Using Nanoimprint Lithography in Combination with Liquid-Phase Epitaxy. *Nanoscale* **2018**, *10*, 18186−18194.
(38) Draine, B. T.; Flatau, P. J. User Guide to the Discrete Dipole Approximation Code DDSCAT (7.3), arXiv:1305.6497v1, arXiv.org e-Print archive.https://arxiv.org/abs/1305.6497 (acessed on 26 May 2013).
(39) Plimpton, S. J. Fast Parallel Algorithms for Short-Range Molecular Dynamics. *Comput. Phys.* **1995**, *117*, 1−19.
(40) Humphrey, W.; Dalke, A.; Schulten, K. VMD: Visual Molecular Dynamics. *J. Mol. Graphics* **1996**, *14*, 33−38.
(41) Johnson, P. B.; Christy, R. W. Optical Constants of the Noble Metals. *Phys. Rev. B* **1972**, *6*, 4370−4379.
(42) Palik, E. D. *Handbook of Optical Constant of Solids*; Academic Press: New York, 1998.
(43) Wu, Y.; Li, G.; Cherqui, C.; Bigelow, N. W.; Thakkar, N.; Masiello, D. J.; Camden, J. P.; Rack, P. D. Electron Energy Loss Spectroscopy Study of the Full Plasmonic Spectrum of Self-Assembled Au−Ag Alloy Nanoparticles: Unraveling Size, Composition, and Substrate Effects. *ACS Photonics* **2016**, *3*, 130−138.
(44) Liu, X.; Li, D.; Sun, X.; Li, Z.; Song, H.; Jiang, H.; Chen, Y. Tunable Dipole Surface Plasmon Resonances of Silver Nanoparticles by Cladding Dielectric Layers. *Sci. Rep.* **2015**, *5*, No. 12555.
(45) Zhang, S.; Bao, K.; Halas, N. J.; Xu, H.; Nordlander, P. Substrate-Induced Fano Resonances of a Plasmonic Nanocube: A Route to Increased-Sensitivity Localized Surface Plasmon Resonance Sensors Revealed. *Nano Lett.* **2011**, *11*, 1657−1663.
(46) Zhu, X.; Zhengmei, Y.; Chen, Y.; Duan, H. Plasmon Modes and Substrate-Induced Fano Dip in Gold Nano-Octahedra. *Plasmonics* **2015**, *10*, 1013−1021.
(47) Hooshmand, N.; Bordley, J. A.; El-Sayed, M. A. Plasmonic Spectroscopy: The Electromagnetic Field Strength and its Distribution Determine the Sensitivity Factor of Face-to-Face Ag Nanocube Dimers in Solution and on a Substrate. *J. Phys. Chem. C* **2015**, *119*, 15579−15587.
(48) Rojas, R.; Claro, F. Electromagnetic Response of an Array of Particles: Normal-Mode Theory. *Phys. Rev. B* **1986**, *34*, 3730−3736.
(49) Pathak, N. K.; Kumar, P. S.; Sharma, R. P. *Noble Metal-Metal Oxide Hybrid Nanoparticles*; Mohapatra, S.; Nguyen, T. A.; Nguyen-Tri, P., Eds.; Elsevier: Duxford, 2018; Vol. *1*, pp 487−498.
(50) Jain, P. K.; El-Sayed, M. A. Surface Plasmon Resonance Sensitivity of Metal Nanostructures: Physical Basis and Universal Scaling in Metal Nanoshells. *J. Phys. Chem. C* **2007**, *111*, 17451−17454.
(51) Wind, M. M.; Vlieger, J.; Bedeaux, D. The Polarizability of a Truncated Sphere on a Substrate. *Phys. A* **1987**, *141*, 33−57.
(52) Rodríguez-Lorenzo, L.; Alvarez-Puebla, R. A.; García de Abajo, F. J.; Liz-Marzan, L. M. Surface Enhanced Raman Scattering Using Star-Shaped Gold Colloidal Nanoparticles. *J. Phys. Chem. C* **2010**, *114*, 7336−7340.
(53) Quan, J.; Zhang, J.; Qi, X.; Li, J.; Wang, N.; Zhu, Y. A Study on the Correlation between the Dewetting Temperature of Ag Flm and SERS Intensity. *Sci. Rep.* **2017**, *7*, No. 14771.
(54) Yurkin, M. A.; Hoekstra, A. G. The Discrete Dipole Approximation: An Overview and Recent Developments. *J. Quant. Spectrosc. Radiat. Transfer* **2007**, *106*, 558−589.
(55) Jain, P. K.; Eustis, S.; El-Sayed, M. A. Plasmon Coupling in Nanorod Assemblies: Optical Absorption, Discrete Dipole Approximation Simulation, and Exciton-Coupling Model. *J. Phys. Chem. B* **2006**, *110*, 18243−18253.
(56) Hooshmand, N.; Panikkanvalappil, S. R.; El-Sayed, M. A. Effects of the Substrate Refractive Index, the Exciting Light Propagation Direction, and the Relative Cube Orientation on the

DOI: 10.1021/acs.jpcc.9b05692
J. Phys. Chem. C 2019, 123, 19879−19886

Plasmonic Coupling Behavior of Two Silver Nanocubes at Different Separations. *J. Phys. Chem. C* **2016**, *120*, 20896−20904.
(57) Chung, T.; Lee, Y.; Ahn, M. S.; Lee, W.; Bae, S. I.; Hwang, C. S. H.; Jeong, K. H. Nanoislands as Plasmonic Materials. *Nanoscale* **2019**, *11*, 8651−8664.
(58) Li, G.; Cherqui, C.; Wu, Y.; Bigelow, N. W.; Simmons, P. D.; Rack, P. D.; Masiello, D. J.; Camden, J. P. Examining Substrate-Induced Plasmon Mode Splitting and Localization in Truncated Silver Nanospheres with Electron Energy Loss Spectroscopy. *J. Phys. Chem. Lett.* **2015**, *6*, 2569−2576.
(59) Kadkhodazadeh, S.; Christensen, T.; Beleggia, M.; Mortensen, N. A.; Wagner, J. B. The Substrate Effect in Electron Energy-Loss Spectroscopy of Localized Surface Plasmons in Gold and Silver Nanoparticles. *ACS Photonics* **2017**, *4*, 251−261.
(60) Neretina, S.; Hughes, R. A.; Gilroy, K. D.; Hajfathalian, M. Noble Metal Nanostructure Synthesis at the Liquid-Substrate Interface: New Structures, New Insights, and New Possibilities. *Acc. Chem. Res.* **2016**, *49*, 2243−2250.
(61) Gilroy, K. D.; Sundar, A.; Hajfathalian, M.; Yaghoubzade, A.; Tan, T.; Sil, D.; Borguet, E.; Hughes, R. A.; Neretina, S. Transformation of Truncated Gold Octahedrons into Triangular Nanoprisms through the Heterogeneous Nucleation of Silver. *Nanoscale* **2015**, *7*, 6827−6835.
(62) Liu, G.; Zhang, C.; Wu, J.; Mirkin, C. A. Using Scanning-Probe Block Copolymer Lithography and Electron Microscopy to Track Shape Evolution in Multimetallic Nanoclusters. *ACS Nano* **2015**, *9*, 12137−12145.
(63) Hajfathalian, M.; Gilroy, K. D.; Hughes, R. A.; Neretina, S. Citrate−Induced Nanocubes: A Reexamination of the Role of Citrate as a Shape−Directing Capping Agent for Ag−Based Nanostructures. *Small* **2016**, *12*, 3444−3452.
(64) Hajfathalian, M.; Gilroy, K. D.; Golze, S. D.; Yaghoubzade, A.; Menumerov, E.; Hughes, R. A.; Neretina, S. A Wulff in a Cage: The Confinement of Substrate-Based Structures in Plasmonic Nanoshells, Nanocages, and Nanoframes Using Galvanic Replacement. *ACS Nano* **2016**, *10*, 6354−6362.
(65) Gilroy, K. D.; Sundar, A.; Farzinpour, P.; Hughes, R. A.; Neretina, S. Mechanistic Study of Substrate-Based Galvanic Replacement Reactions. *Nano Res.* **2014**, *7*, 365−379.

DOI: 10.1021/acs.jpcc.9b05692
J. Phys. Chem. C 2019, 123, 19879−19886